

# Processing and characterization of UHMWPE composite fibres with alumina particles in poly(ethylene-vinyl acetate) matrix

Journal of Thermoplastic Composite  
Materials

2018, Vol. 31(5) 689–708

© The Author(s) 2017

Reprints and permissions:

sagepub.co.uk/journalsPermissions.nav

DOI: 10.1177/0892705717718240

journals.sagepub.com/home/jtc



Jelena Zec<sup>1</sup>, Nataša Tomić<sup>2</sup>, Milorad Zrilić<sup>1</sup>, Smilja Marković<sup>3</sup>,  
Dušica Stojanović<sup>1</sup> and Radmila Jančić-Heinemann<sup>1</sup>

## Abstract

Processing of hybrid composites represents a challenge for engineers where the aim is to establish compatibility among several materials. The aim of this study is to evaluate the effects of different sizes and morphologies of alumina fillers on the mechanical and thermal properties of the composite fibres based on ultra-high molecular weight polyethylene fibres (UHMWPE). These fibres have an outstanding elastic modulus and they are compatible with nonpolar sequences of the poly(ethylene-co-vinyl acetate) (EVA) matrix. Compared to the fibres, inferior mechanical properties of the matrix can be improved using alumina particles. Commercial aluminium oxide ( $\text{Al}_2\text{O}_3$ ) nanoparticles, commercial whiskers and synthesized particles of  $\text{Al}_2\text{O}_3$  doped with iron oxide, incorporated in different weight percentages, were used as fillers. The UHMWPE fibres were impregnated using the solution of EVA in toluene with dispersed particles. Fourier transform infrared spectroscopy and field emission scanning electron microscope were used for structural examination. Tensile testing revealed increasing of modulus of elasticity and strengths of obtained hybrid composite fibres. Thermal gravimetry showed improved thermal stability up to  $350^\circ\text{C}$  of the hybrid composite fibres with alumina particles doped with iron oxide. Results of tested samples showed that the best

<sup>1</sup> University of Belgrade, Faculty of Technology and Metallurgy, Belgrade, Serbia

<sup>2</sup> Innovation Center of Faculty of Technology and Metallurgy, University of Belgrade, Belgrade, Serbia

<sup>3</sup> Institute of Technical Sciences of SASA, Belgrade, Serbia

## Corresponding author:

Nataša Tomić, Innovation Center of Faculty of Technology and Metallurgy, University of Belgrade, Belgrade, Serbia.

Email: ntomic@tmf.bg.ac.rs

mechanical properties were for hybrid composite fibres with 1 wt% of iron doped alumina filler.

### **Keywords**

UHMWPE, Al<sub>2</sub>O<sub>3</sub> reinforcement, EVA matrix, hybrid composite fibres, thermal stability

## **Introduction**

Fibre-reinforced polymer composites are widely used due to their excellent properties, such as light weights, high tensile strength and moduli.<sup>1</sup> Poly(ethylene-co-vinyl acetate) (EVA) is a random copolymer synthesized by the copolymerization of ethylene and vinyl acetate monomers with different acetate contents.<sup>2</sup> Due to their properties and processing characteristics, these copolymers have extensive applications in biomedical, food industry, construction, transport, wire and cable industry. They are commonly used as adhesives, electrical insulation, corrosion protection, waterproofing and packaging.<sup>2-4</sup> EVA copolymers are often used as adhesives in combination with different types of materials like wood, rubber, metals, glass and polymers.<sup>5,6</sup> EVA properties depend on the content of each comonomer. Crystallization and melting characteristics of EVA are very sensitive to the VA content.<sup>7</sup> The melting temperature and degree of crystallinity decreases with an increase of vinyl acetate groups, but the glass transition temperature ( $T_g$ ) increases with the increase of vinyl acetate content.<sup>5-8</sup> The presence of ethylene segments in EVA molecules provides characteristic to 'plasticized' and increases the activity.<sup>9</sup>

The mechanical properties of the EVA as matrix are inferior compared to the fibres like ultra-high molecular weight polyethylene (UHMWPE) and they can be improved using inorganic fillers having a different morphology. The main reason to incorporate inorganic particles into polymer matrices is to obtain a composite with improved mechanical properties like tensile strength, hardness, Young's modulus or stiffness by applying different reinforcement mechanisms.<sup>10</sup>

A material that is widely used in composites is UHMWPE with long chains that provide sufficient load transfer between the macromolecules.<sup>11</sup> Due to its wear resistant characteristics, chemical inertness, strength, high impact resistance, toughness, tensile strength and excellent modulus, it has become one of the most modified polymers.<sup>12</sup> The most significant characteristics include high specific fibre strength that is about 15 times stronger than steel. These advancements have led to the development of high-performance polymer matrix composites.<sup>13</sup> The combination of high tensile strength, stiffness, low density and damage tolerance made UHMWPE fibres an ideal material. Ropes and cables made of this material have various applications for kites, fishing lines, offshore mooring and so on.<sup>11</sup> The extreme tensile strength and the possibility to apply thick cables allow overdesign of the cable up to load carrying capacity of a few tons.

UHMWPE fibres have lack polarity and, therefore, it is not easy to produce composites due to the poor interfacial bonding with the matrix. On the other side, lateral interactions between molecules are the result of van der Waals forces. Their presence in

composite materials helps in transferring off-axis loads retaining good mechanical properties along the fibre axis.<sup>14</sup> Although UHMWPE fibres have numerous useful characteristics and provide a load-bearing effect, their weakness is poor thermal resistance. In hybrid composite fibres, the function of polymer is to transfer load to the reinforcement and protect it from chemical and high-temperature influences.<sup>15</sup> For this purpose, the most commonly used thermosetting resins are epoxy, but brittle, low impact resistance and low toughness limit their usage. Weaknesses of epoxy resins can be overcome with the incorporation of the reinforcement phase such as UHMWPE fibres.<sup>16</sup>

In order to investigate the behaviour of materials with different fillers, considerable studies have been conducted. That includes zirconium particles, TiO<sub>2</sub>, kaolin, aluminium oxide (Al<sub>2</sub>O<sub>3</sub>), carbon fibres, carbon nanotubes and so on.<sup>12</sup> Combination of organic and inorganic components and obtaining new materials attract increasing attention, since they combine the properties of including constituents.<sup>17</sup>

Jin et al. have studied the composites where EVA is used as the polymer matrix and alumina nanoparticles as fillers. There was no agglomeration for 1.5 wt% of Al<sub>2</sub>O<sub>3</sub> nanoparticles. The influence of the Al<sub>2</sub>O<sub>3</sub> content on the tensile strength of EVA/Al<sub>2</sub>O<sub>3</sub> nanocomposites showed increasing values up to 1.5 wt% of Al<sub>2</sub>O<sub>3</sub> and at a higher content, the tensile strength starts to decrease, probably due to the agglomeration of nanoparticles.<sup>18</sup> Baskaran et al.<sup>19</sup> studied the effect of alumina nanoparticles in the mechanical properties of the nanocomposites. Chee et al.<sup>20</sup> noticed that the higher amount of alumina nanoparticles would reduce the reinforcing effect and mechanical properties of the composite due to poor dispersion and agglomeration.

In this work, different alumina fillers have been chosen due to their specific properties, including hardness, wear resistance, high elastic modulus, thermal stability, high adsorption capacity, good thermal conductivity, high strength and stiffness and good resistance to chemical and thermal environments.

Al<sub>2</sub>O<sub>3</sub> has several crystal forms, and corundum is one of the most desired form for the reinforcement of composite materials when mechanical properties are important. Considering that  $\alpha$ -Al<sub>2</sub>O<sub>3</sub> is the hardest form of alumina, it was a good choice to be used as reinforcement in order to improve the mechanical and thermal properties of polymer matrix composites. Like the other metal oxides, when Al<sub>2</sub>O<sub>3</sub> is exposed to the atmosphere, its surface becomes covered with water in the form of the terminal OH groups.<sup>21</sup> Fine alumina particles exert influence on mechanical properties of the composite, even if the quantity is rather small.<sup>22</sup> Opelt et al. reported that after the addition of 0.15, 0.50 and 1.50 wt% of alumina, the modulus of elasticity had increased, respectively. For tensile strength, the results showed that there is no significant variation between the neat matrix and nanocomposite with small amount of Al<sub>2</sub>O<sub>3</sub> fillers.<sup>23</sup> According to Wetzel et al., the similar behaviour is observed for nanocomposites with up to 1% volume fraction (approximately 3.5 wt%) of alumina fillers. On the other hand, flexural modulus and strength depend on the filler volume fraction.<sup>24</sup>

Particle sizes at micro-scale have a low influence on Young's modulus. However, at nanoscale, Young's modulus of the composite increases as the size of particles decreases. It was also reported that tensile strength decreases in composites with 3 vol.% nanoparticles, due to poor dispersion. Conversely, at 1 vol.% loading of microparticles,

the tensile strength increases.<sup>25</sup> In the case of the  $\text{Al}_2\text{O}_3$ /epoxy nanocomposites, the formation of an interconnected network formed by the alumina nanoparticles was given as the main reason for the elastic modulus enhancements.<sup>26</sup> However, the elastic modulus in nanocomposites does not increase continuously with increasing the weight percentage of fillers. After the optimum weight percentage is reached, due to stress concentration, the elastic modulus will decrease.<sup>27</sup>

The aim of the present work is to research the properties of UHMWPE hybrid composite in EVA matrix modified by commercial nanoparticles and whiskers of  $\text{Al}_2\text{O}_3$  as fillers and comparing the properties of composite in case of using new synthesized particles of alumina doped with iron oxide. Based on the results, the application of the hybrid composite material with the best characteristics will also be examined.

## Experimental

### Materials

The polyethylene used in this study was UHMWPE – DSM Dyneema, The Netherlands (SK75; filament diameter 20  $\mu\text{m}$ ; density 0.970  $\text{g cm}^{-3}$ ). Commercial EVA (Elvax<sup>®</sup> 410) produced by DuPont<sup>™</sup>, containing 18 wt% of vinyl acetate, was chosen as a polymer matrix. Commercial toluene (produced by Zorka Šabac) was used as a solvent. The aluminium oxide nanoparticles (<50 nm particle size) and alumina whiskers (diameter 2–4 nm  $\times$  400 nm) were commercially supplied from Sigma Aldrich, USA. Aluminium chloride hydroxide (Locron L) was purchased from the Clariant Company in the crystallized state of  $\text{Al}_2\text{Cl}(\text{OH})_5 \cdot 2.5 \cdot \text{H}_2\text{O}$ . This product contained 23.5%  $\text{Al}_2\text{O}_3$  and 8.18% Cl, corresponding to an Al/Cl molar ratio of 2/1. Iron chloride ( $\text{FeCl}_3$ ) was also purchased from the same company.

### Methods

Alumina particles doped with iron oxide were synthesized via sol-gel technique by the hydrolysis of aluminium ion. Solution of aluminium chloride hydroxide and  $\text{FeCl}_3$  in water was mixed in a weight ratio of 19.5 g  $\text{Al}_2(\text{OH})_5\text{Cl}$ , 0.5 g  $\text{FeCl}_3$  and 15 g  $\text{H}_2\text{O}$ . Obtained gel was calcined for 2 h at 900°C.<sup>28</sup> The mixture was grinded in a mortar and then sifted through a sieve. Nanoparticles, whiskers and synthesized particles of  $\text{Al}_2\text{O}_3$  doped with iron oxide were annotated as n- $\text{Al}_2\text{O}_3$ , w- $\text{Al}_2\text{O}_3$  and Fe- $\text{Al}_2\text{O}_3$ . Obtained hybrid composite fibres with iron doped particles, alumina nanoparticles and alumina whiskers in UHMWPE fibres hybrid composite in EVA matrix were annotated as 1Fe- $\text{Al}_2\text{O}_3$ /EVA/UHMWPE, 3Fe- $\text{Al}_2\text{O}_3$ /EVA/UHMWPE, 5Fe- $\text{Al}_2\text{O}_3$ /EVA/UHMWPE, 1n- $\text{Al}_2\text{O}_3$ /EVA/UHMWPE, 3n- $\text{Al}_2\text{O}_3$ /EVA/UHMWPE, 5n- $\text{Al}_2\text{O}_3$ /EVA/UHMWPE, 1w- $\text{Al}_2\text{O}_3$ /EVA/UHMWPE, 3w- $\text{Al}_2\text{O}_3$ /EVA/UHMWPE and 5w- $\text{Al}_2\text{O}_3$ /EVA/UHMWPE for the addition of 1, 3 and 5 wt% of the particles, respectively.

To obtain solutions with 1, 3 and 5 wt% of fillers, n- $\text{Al}_2\text{O}_3$ , w- $\text{Al}_2\text{O}_3$  and Fe- $\text{Al}_2\text{O}_3$  were added in toluene. Uniform dispersion of particles was achieved after 1 h in ultrasound bath. Afterwards, 20 wt% of EVA was added into prepared solution and mixed at 60°C with the magnetic stirrer at a rotation speed of 500 r/min for 1 h. Prepared mixtures

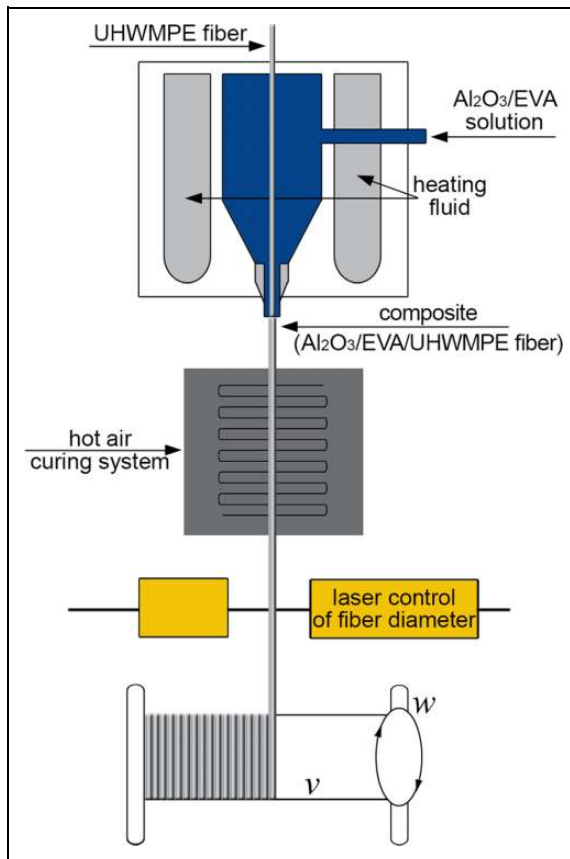


**Figure 1.** Schematic presentation of UHMWPE impregnation process. UHMWPE: ultra-high molecular weight polyethylene.

were used for UHMWPE fibre impregnation using apparatus showed in Figure 1.<sup>29</sup> The nozzle was changed and its dimensions were  $0.4 \times 1.5 \text{ mm}^2$ , adapted to the dimensions of the fibres that are impregnated. To avoid composite sticking on a drum, impregnated fibres were cured with hot air at  $60^\circ\text{C}$  before winding.

### Characterization

The distribution of the filler particles was determined using an optical microscope and the laser particle size analyzer (PSA) Mastersizer 2000 (Malvern Instruments Ltd., UK).

Morphology and shape of the particles were observed using a Mira3 Tescan field emission scanning electron microscope (FE-SEM [Tescan Ltd., UK]), operated at 20 kV. The samples were previously coated with a thin gold film. The particle size and the dispersion of synthesized fillers were obtained by image analysis using the Image Pro

Plus 6.0 software. Images from FE-SEM were further used for measuring diameters, particle size distribution and particle shape characterization. The laser PSA Mastersizer 2000 was used to measure the particle size distribution, which covers the particle size range of 0.02–2000  $\mu\text{m}$ .

The chemical structure of the samples was analyzed using a Fourier transform infrared (FTIR) spectroscopy at Nicolet 6700 spectrometer from Thermo Fisher Scientific Inc., USA, in the attenuated total reflectance (ATR) mode with a single bounce 45° Golden Gate ATR accessory with a diamond crystal and an electronically cooled deuterated triglycine sulfate (DTGS) detector (Thermo Fisher Scientific Inc., USA). The spectra were the co-addition of 64 scans at 4  $\text{cm}^{-1}$  spectral resolution and ATR corrected. The spectrometer was equipped with OMNIC 9 software and recorded the spectra in the wavelength range from 2.5  $\mu\text{m}$  to 20  $\mu\text{m}$ . Infrared spectra were recorded in transmission mode between 400  $\text{cm}^{-1}$  and 4000  $\text{cm}^{-1}$ . Fourier transform, as a mathematical process, was required to convert the raw data into the actual spectrum.

Thermal analyses of samples were conducted by using a differential scanning calorimetry (DSC) and thermogravimetric analysis (TGA). The DSC measurements were conducted using a TA DSC Q10 (TA Instruments, USA) calibrated with indium standards. The temperature range was from 30°C to 180°C at a heating rate of 10°C  $\text{min}^{-1}$  with a dynamic nitrogen flow of 50  $\text{ml min}^{-1}$ . The samples were heated up to 180°C, kept at 180°C for 5 min to erase thermal history and cooled down to 30°C at the same cooling rate. A second heating was done on the each sample. The TGA was performed on a TGA/STD Q600 (TA Instruments, USA) under a nitrogen gas flow (100  $\text{ml min}^{-1}$ ) between 30°C and 600°C with a heating rate of 10°C  $\text{min}^{-1}$ .

The tensile strength of the samples was examined using a servo hydraulic, mechanical testing machine INSTRON 1332 (Instron Ltd., USA) with control electronics FASTtrack 8800. Strain rate was 5  $\text{mm min}^{-1}$ . All samples were of the same length and three replicates of each sample were used in the testing procedure.

## **Results and discussion**

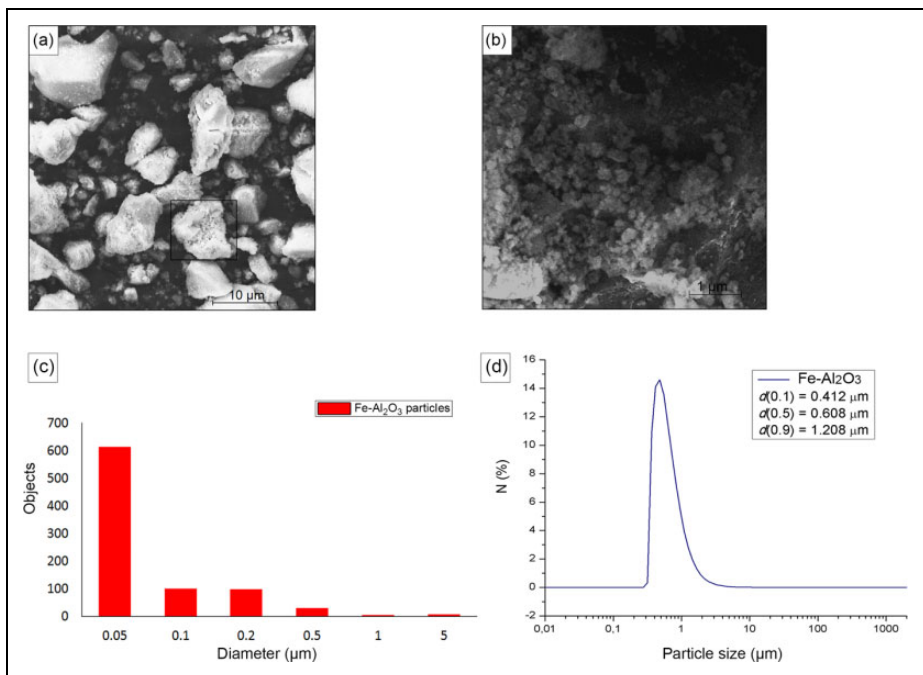
The displayed measurement and results were performed in order to determine which filler contributes the most to the mechanical properties of the hybrid composite EVA/UHMWPE.

### *The distribution of particles*

Analyzing the images from the FE-SEM and processing by Image Pro Plus software, the distribution of alumina particles doped with iron oxide ( $\text{Fe-Al}_2\text{O}_3$ ) particle dimension showed submicron range of diameters achieved by the sol-gel technique. More than 850 objects were analyzed in every sample of particles using the automatic object recognition algorithm. The average diameter of 0.15  $\mu\text{m}$  (Table 1) was determined as most of the objects had very small dimensions. A few agglomerates have been noticed (Figure 2(a)) as the result of lower dispersion of the particles and their joining during the calcination process, but they were recognized as individual objects by the algorithm. The presence of

**Table 1.** Statistical data of particle size distribution obtained by the image analysis of Fe-Al<sub>2</sub>O<sub>3</sub>.

Sample		Area	Max diameter (μm)	Min diameter (μm)	Mean diameter (μm)	Roundness
Fe-Al <sub>2</sub> O <sub>3</sub>	Min	0.0032	0.0565	0.0565	0.0565	1.000
	Max	542.134	55.068	12.942	26.745	176.455
	Mean	0.966	0.239	0.103	0.150	1.542
	Standard deviation	201.418	23.139	0.530	1.093	8.341

**Figure 2.** (a) FE-SEM micrograph of Fe-Al<sub>2</sub>O<sub>3</sub>, (b) magnified part of Fe-Al<sub>2</sub>O<sub>3</sub>, FE-SEM micrograph, (c) statistical distribution of Fe-Al<sub>2</sub>O<sub>3</sub>, – diameter and (d) particle size distribution of Fe-Al<sub>2</sub>O<sub>3</sub>. FE-SEM: field emission scanning electron microscope.

particle aggregates was reflected by high values of maximal observed particle diameters in Table 1. The predominance of a great number of particles with low diameters (obvious on Figure 2(b)) led to small mean diameter of particles, as can be seen in Figure 2(c). The range of measured objects is even larger than presented in Figure 2(c) where it was between 0 μm and 5 μm, but the very large objects were agglomerates that are dissipated

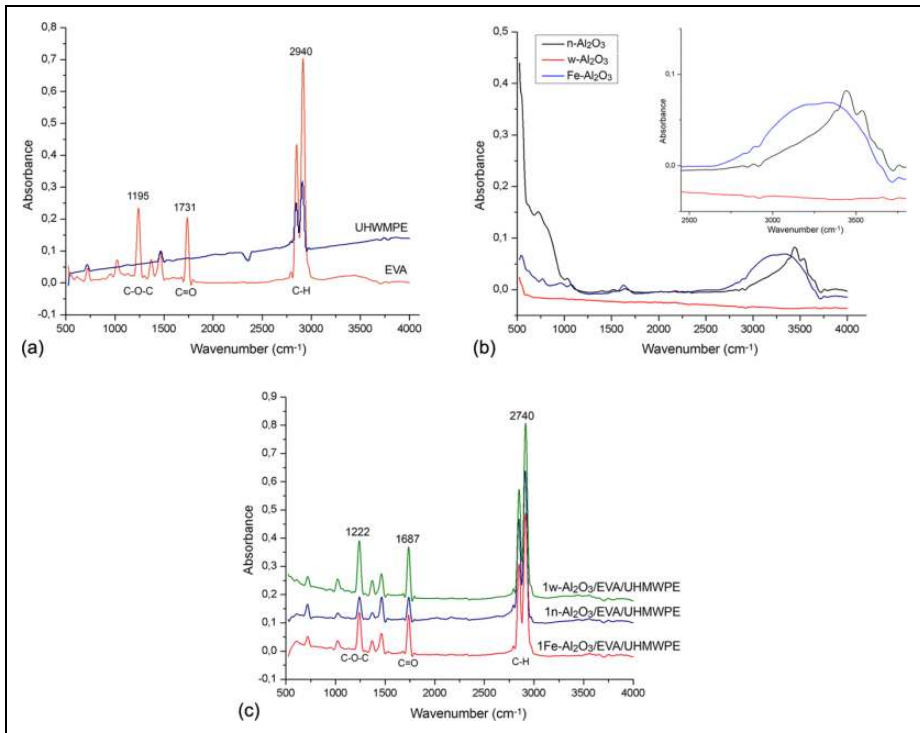


**Figure 3.** FTIR spectra for fillers and hybrid composite fibres: (a) EVA/UHMWPE, (b)  $n\text{-Al}_2\text{O}_3$ ,  $w\text{-Al}_2\text{O}_3$  and  $\text{Fe-Al}_2\text{O}_3$ , and (c)  $1n\text{-Al}_2\text{O}_3/\text{EVA/UHMWPE}$ ,  $1w\text{-Al}_2\text{O}_3/\text{EVA/UHMWPE}$  and  $1\text{Fe-Al}_2\text{O}_3/\text{EVA/UHMWPE}$  hybrid composite fibres.

$\text{Al}_2\text{O}_3$ : aluminium oxide; FTIR: Fourier transform infrared; EVA: poly(ethylene-co-vinyl acetate); UHMWPE: ultra-high molecular weight polyethylene.

on smaller particles in the processing of the composite so the most important information is the mean value of observed individual particles.

Particle size distribution indicated a narrow distribution of  $\text{Fe-Al}_2\text{O}_3$  in the interval between  $0.3\ \mu\text{m}$  and  $1.3\ \mu\text{m}$ , with a maximum peak at  $0.48\ \mu\text{m}$  (Figure 2(d)). The obtained values for particle size were in accordance with the range of distribution of mean diameter (Figure 2(c)) suggesting that the most of agglomerates dissipated on single submicron particles.

### ATR-FTIR analysis

Chemical structure and interactions were examined using FTIR. Spectra of the  $n\text{-Al}_2\text{O}_3$ ,  $w\text{-Al}_2\text{O}_3$  and  $\text{Fe-Al}_2\text{O}_3$  are given in Figure 3.



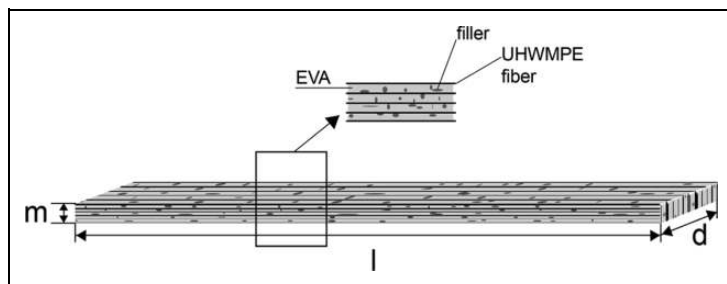


**Figure 4.** Dimensions of the samples.

FTIR identifies chemical bonds in a molecule of organic and inorganic samples by producing an infrared absorption spectrum. The resulting spectrum represents the molecular absorption and creates a molecular fingerprint of the sample.

The scope of interest was acetate ( $1195\text{ cm}^{-1}$ ), carbonyl ( $1731\text{ cm}^{-1}$ ) and ethylene sequence C–H ( $2940\text{ cm}^{-1}$ ) absorption region of the IR spectrum for EVA (Figure 3(a)). The UHMWPE fibres showed characteristic absorption of ethylene segments ( $1470$ ,  $2950/2920$  and  $720\text{ cm}^{-1}$ ).

Spectra for n- $\text{Al}_2\text{O}_3$ , w- $\text{Al}_2\text{O}_3$  and Fe- $\text{Al}_2\text{O}_3$  fillers (Figure 3(b)) showed changes in the intensities of absorption bands at  $3300\text{ cm}^{-1}$  that was attributed to the presence of the O–H groups. The peak intensity of O–H groups for n- $\text{Al}_2\text{O}_3$  and Fe- $\text{Al}_2\text{O}_3$  indicated that these groups were present in a greater content on the surface than w- $\text{Al}_2\text{O}_3$ . The function of these groups was to establish a better bonding with the composite.

The FTIR spectra for 1n- $\text{Al}_2\text{O}_3/\text{EVA}/\text{UHMWPE}$ , 1w- $\text{Al}_2\text{O}_3/\text{EVA}/\text{UHMWPE}$  and 1Fe- $\text{Al}_2\text{O}_3/\text{EVA}/\text{UHMWPE}$  (Figure 3(c)) indicated the characteristic peaks at  $1222$ ,  $1687$  and  $2740\text{ cm}^{-1}$  that referred to the presence of C–O–C, C=O and C–H groups, respectively. Also, no vibrations of the O–H groups were noted. This indicated that these groups were used for establishing the hydrogen bonds between particles and EVA/UHMWPE hybrid composite fibres.

### FE-SEM analysis

In this study, EVA/UHMWPE was compounded with the same proportions (1 wt%) of different particles. Based on the FE-SEM images, the surface properties of the fillers, matrix and UHMWPE fibre, as reinforcement, were analyzed. Dimensions of the samples (Figure 4) were length ( $l$ )  $30 (\pm 0.1)$  mm; width ( $d$ )  $1.5 (\pm 0.05)$  mm; and thickness ( $m$ )  $0.43 (\pm 0.03)$  mm. The mass proportion of UHMWPE fibres, EVA and particles in the matrix was 48.09, 51.91 and 0.52 wt%, respectively.

In order to obtain an insight into the impregnation quality, the cross section of the sample was made by a sharp medical blade. To examine the morphology and the type of failure, the fractured surfaces of the samples after the tensile test were sputtered with gold and observed under SEM.

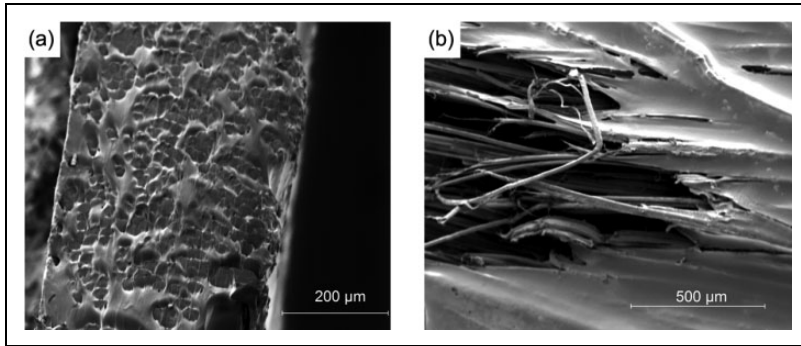


**Figure 5.** The FE-SEM micrograph of unmodified EVA/UHMWPE composite: (a) cross section before tensile test and (b) surface of composite breakage.

FE-SEM: field emission scanning electron microscope; EVA: poly(ethylene-co-vinyl acetate); UHMWPE: ultra-high molecular weight polyethylene.

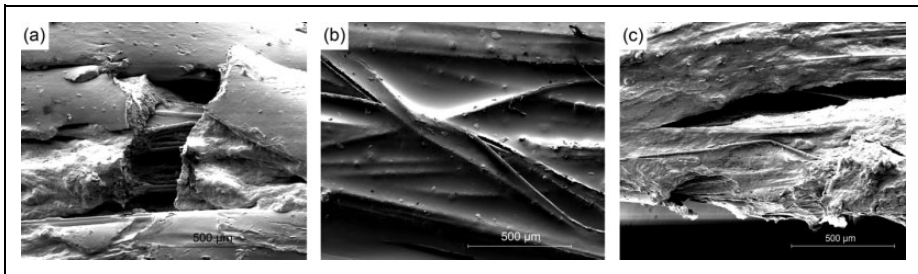


**Figure 6.** The FE-SEM micrograph of EVA/UHMWPE composite with: (a)  $n\text{-Al}_2\text{O}_3$ , (b)  $w\text{-Al}_2\text{O}_3$  and (c)  $\text{Fe-Al}_2\text{O}_3$ .

FE-SEM: field emission scanning electron microscope; EVA: poly(ethylene-co-vinyl acetate); UHMWPE: ultra-high molecular weight polyethylene;  $\text{Al}_2\text{O}_3$ : aluminium oxide.

The FE-SEM pattern of a fractured surface of EVA/UHMWPE composite is shown in Figure 5.

Cross-sectional view in Figure 5(a) showed that the fibre distribution in matrix was uniform, as well the wetting of UHMWPE fibres, which means that these fibres were a proper choice for EVA reinforcement due to established adhesion between these components. FE-SEM micrograph in Figure 5(b) showed thinned UHMWPE fibres that acted as a main load bearing element. Good adhesion of EVA matrix to the fibres enabled simultaneous elongation of both components as a response to the applied load, which was followed by ductile fracture of the EVA/UHMWPE composite. Fractured surfaces of EVA/UHMWPE composite with  $n\text{-Al}_2\text{O}_3$ ,  $w\text{-Al}_2\text{O}_3$  and  $\text{Fe-Al}_2\text{O}_3$  particles are shown in Figure 6.

SEM image after the tensile test of EVA/UHMWPE hybrid composite fibres with  $\text{Al}_2\text{O}_3$  nanoparticles (Figure 6 (a)) showed a brittle fracture. The transverse fracture

surface of the matrix indicated the combined effect of mechanical interlocking between fibres and matrix with  $1n\text{-Al}_2\text{O}_3$ . Better fibre–matrix interfacial bonding and propagation resistance across the cross sections of samples resulted in higher strengths in hybrid composite fibres. This image was in accordance with the tensile stress results due to their higher resistance compared to the unmodified composite and  $w\text{-Al}_2\text{O}_3/\text{EVA}/\text{UHMWPE}$ .

Poor interfacial adhesion between the UHMWPE fibres and matrix is shown in Figure 6. The whiskers did not sufficiently strengthen the matrix and the fibres were pulled out. Agglomeration and segregation of whiskers were also detected. According to a separate pulled out fibre, it could be concluded that the connection between fibre and matrix was weak. The separation at the fibre–matrix interface indicated that the longitudinal cracks were nucleated at this interface.

The FE-SEM micrograph of fractured surfaces of  $\text{Fe-Al}_2\text{O}_3/\text{EVA}/\text{UHMWPE}$  showed longitudinal cracking of EVA with improved interfacial adhesion and mechanical properties of the hybrid composite fibres that caused cohesive failure of the matrix (Figure 6(c)). It could be seen that the EVA covered the surface of UHMWPE fibres that led to higher interactions between the surfaces of the composite components.

### DSC analysis

The difference in melting temperature is one of the essential indicators for the required demands of studied composites. DSC as a calorimetry method measures heat flow as a function of temperature. Heat flow can indicate structural changes driven by thermal processes. At the same time, it is a good indicator of thermal active transitions, such as melting temperature and glass transition temperature. DSC thermograms of samples are shown in Figure 7. From the represented thermogram, it was noticed only one melting peak for neat EVA and UHMWPE fibres at  $78.4^\circ\text{C}$  and  $137.2^\circ\text{C}$ , respectively.

For UHMWPE fibres, a slight difference in melting temperature ( $T_m$ ) between obtained and the one reported by the producer ( $144\text{--}152^\circ\text{C}$ ) was shown due to the environmental and storage conditions like humidity, increased storage temperature, DSC set parameters and so on.<sup>30</sup> EVA copolymer is a partially crystalline polymer that consists of crystalline ethylene segments and also a non-crystalline (amorphous) vinyl acetate segments.<sup>7</sup> An endothermic peak was typical for crystal melting of ethylene sequences in EVA copolymer,<sup>31</sup> which was low ( $\Delta H_{m1} = 8.708 \text{ J g}^{-1}$ ), Table 2. Unlike EVA and UHMWPE fibres, composites exhibited two clearly separated endothermic peaks corresponding to the melting phase transition of EVA and UHMWPE components. The endothermic effects were quantified by determining the total enthalpy change from the peak area for the different samples (Table 2). A significant change for neat EVA was observed at around  $78^\circ\text{C}$ . According to Badiie et al.,<sup>32</sup> it can be associated with internal structural changes or crystallization transitions of the matrix.

The addition of fillers reduced the melting enthalpy of UHMWPE fibres. Compared to the melting temperature of neat EVA, fillers slightly increased the melting temperature of the matrix (2.2%). When the melting point of EVA/UHMWPE and hybrid composites were compared, it can be concluded that no change in melting point was observed by inducing particles. The main change in EVA phase melting transition was

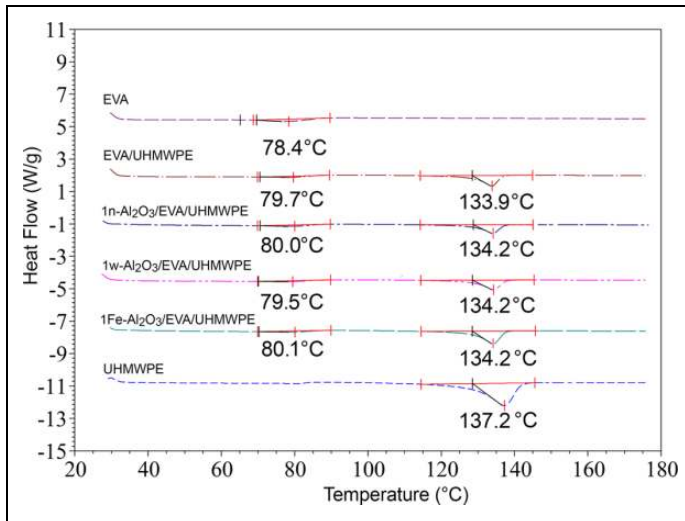


**Figure 7.** DSC thermograms of EVA, UHMWPE fibres and composite fibres. DSC: differential scanning calorimetry; EVA: poly(ethylene-co-vinyl acetate); UHMWPE: ultra-high molecular weight polyethylene.

**Table 2.** Temperatures and enthalpies obtained from DSC thermograms.

Samples	$T_{m1}$ (°C; EVA phase)	$\Delta H_{m1}$ (J g <sup>-1</sup> ; EVA phase)	$T_{m2}$ (°C; UHMWPE phase)	$\Delta H_{m2}$ (J g <sup>-1</sup> ; UHMWPE phase)
UHMWPE			137.2	78.2
EVA	78.4	8.7		
EVA/UHMWPE	79.7	3.6	133.8	24.7
1n-Al <sub>2</sub> O <sub>3</sub> /EVA/ UHMWPE	80.0	4.1	134.2	20.9
1w-Al <sub>2</sub> O <sub>3</sub> /EVA/ UHMWPE	79.5	3.0	134.2	24.4
1Fe-Al <sub>2</sub> O <sub>3</sub> /EVA/ UHMWPE	80.1	3.3	134.2	32.3

DSC: differential scanning calorimetry; Al<sub>2</sub>O<sub>3</sub>: aluminium oxide.

noticed by melting enthalpy. Sharp decrease in melting enthalpy ( $\Delta H_{m1}$ ) for 52.9–65.5% suggested large-scale structural changes due to the disturbance of polyethylene segment packing by the introduction of reinforcement as UHMWPE and particles. Maintained value for  $T_{m1}$  enabled preserved mechanical properties of EVA matrix concerning the elongation of the composites and the amount of absorbed load.

However, a change of the melting temperature of UHMWPE phase did not follow specific order and the values for hybrid composite were similar. Melting enthalpy of UHMWPE phase for hybrid composites showed significant differences. The highest

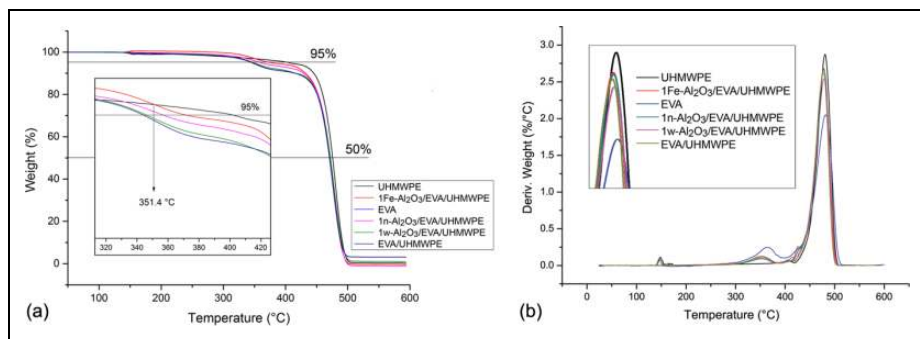


**Figure 8.** TG (a) and DTG (b) diagrams for EVA, UHMWPE fibres and hybrid composite fibres. EVA: poly(ethylene-co-vinyl acetate); UHMWPE: ultra-high molecular weight polyethylene.

melting enthalpy of UHMWPE phase ( $\Delta H_{m2}$ ) for hybrid composite 1Fe- $\text{Al}_2\text{O}_3$ /EVA/UHMWPE showed the structural arrangement of reinforcement. Negligible UHMWPE melting point decrement (2.2%) in composites may be prescribed to structural changes due to the disturbance of surface polyethylene sequences by the processing of hybrid composites, and thus, the use value of composites was not affected by the use of presented technology.

Overall endothermic enthalpy for six samples was classified in the following rank: UHMWPE ( $78.2 \text{ J g}^{-1}$ ) > 1Fe- $\text{Al}_2\text{O}_3$ /EVA/UHMWPE ( $35.6 \text{ J g}^{-1}$ ) > EVA/UHMWPE ( $28.3 \text{ J g}^{-1}$ ) > 1w- $\text{Al}_2\text{O}_3$ /EVA/UHMWPE ( $27.4 \text{ J g}^{-1}$ ) > 1n- $\text{Al}_2\text{O}_3$ /EVA/UHMWPE ( $24.9 \text{ J g}^{-1}$ ) > EVA ( $8.7 \text{ J g}^{-1}$ ).

### Thermal degradation study of hybrid composite fibres

Thermogravimetric (TG) curves and derivative TG curves (DTG) of EVA, UHMWPE fibres and composites are presented in Figure 8(a). Thermal stability was evaluated at decomposition temperatures at 5% of weight loss ( $T_{0.05}$ ) and at 50% of weight loss ( $T_{0.5}$ ).

Degradation of EVA, as the matrix, was followed by two degradation steps. The first step was a deacetylation process that started at  $286.5^\circ\text{C}$  and completed at  $381.5^\circ\text{C}$ . In this temperature range, chain fragments as carbon monoxide, carbon dioxide ketene and water were probably formed during the thermal decomposition of the acetic acid.<sup>33</sup> Within this interval, EVA yielded ethylene and acetic acid.<sup>34</sup>

At the first point ( $T_{0.05}$ ), the highest temperature of degradation that occurred for UHMWPE fibres and 1Fe- $\text{Al}_2\text{O}_3$ /EVA/UHMWPE was  $408.1^\circ\text{C}$  and  $383.3^\circ\text{C}$ , respectively. From  $156.6^\circ\text{C}$  to  $351.4^\circ\text{C}$  interval, 1Fe- $\text{Al}_2\text{O}_3$ /EVA/UHMWPE showed higher stability than other samples.

On the second point ( $T_{0.5}$ ), all the samples displayed similar degradation profiles. The second step referred to the degradation of the EVA backbone (chain scission within the interval of  $400\text{--}500^\circ\text{C}$ ).<sup>35,36</sup> It was noticeable that the presence of fillers in EVA improved the thermal stability of the matrix. According to the results presented in Table 3, decomposition temperatures  $T_{0.05}$  and  $T_{0.5}$  showed that the reinforcement of EVA

**Table 3.** Temperatures obtained from TG/DTG diagrams.

Samples	TG			DTG	
	$T_{0.05}$ (°C)	$T_{0.5}$ (°C)	Mass residual (%)	$T_1$ (°C)	$T_2$ (°C)
UHMWPE	408.1	477.5	0.421		480.9
EVA	347.6	471.1	3.277	364.1	481.6
EVA/UHMWPE	345.7	471.7	3.243	352.3	477.2
1n-Al <sub>2</sub> O <sub>3</sub> /EVA/UHMWPE	357.1	471.8	0.009	352.9	478.4
1w-Al <sub>2</sub> O <sub>3</sub> /EVA/UHMWPE	349.5	472.7	1.154	351.6	480.8
1Fe-Al <sub>2</sub> O <sub>3</sub> /EVA/UHMWPE	383.3	472.4	0.110	351.6	478.5

UHMWPE: ultra-high molecular weight polyethylene; EVA: poly(ethylene-co-vinyl acetate); Al<sub>2</sub>O<sub>3</sub>: aluminium oxide.

matrix improved the thermal stability.<sup>30</sup> The experimental results (Figure 8(a)) showed that the addition of fillers improved thermal stability and prolonged degradation temperatures.

The higher mass residual for neat EVA (3.27%) was associated with networking of EVA polymer due to instability and formation of double bonds after the degradation. Costache et al. suggested that, in the first step of degradation, acetic acid loss was related to the presence of hydroxyl groups on the edges of fillers,<sup>37</sup> which was in accordance with the results obtained for neat EVA. Results for hybrid composite fibres proved that the lowest mass weight loss was for 1n-Al<sub>2</sub>O<sub>3</sub>/EVA/UHMWPE and 1Fe-Al<sub>2</sub>O<sub>3</sub>/EVA/UHMWPE. Degradation processes of EVA matrix, UHMWPE fibres and UHMWPE/EVA hybrid composite fibres were represented by DTG curves in Figure 8(b). For all samples except UHMWPE fibres, degradation occurred at approximately 351°C. The final point was similar for all samples and it is shown in Table 3.

### Tensile test

Tests were performed in order to determine tensile strength and modulus of elasticity of EVA/UHMWPE hybrid composite fibres with different fillers and their mass fractions.

The values of tensile strength of different concentrations of fillers are presented in Figure 9. The highest values for different fillers and concentrations were for 1Fe-Al<sub>2</sub>O<sub>3</sub>/EVA/UHMWPE (823.02 MPa).

According to the results given in Figure 9, the dependence of tensile stress on the relative displacement of four samples of 1n-Al<sub>2</sub>O<sub>3</sub>/EVA/UHMWPE, 1w-Al<sub>2</sub>O<sub>3</sub>/EVA/UHMWPE, 1Fe-Al<sub>2</sub>O<sub>3</sub>/EVA/UHMWPE and EVA was presented in Figure 10. The addition of 1 wt% of any of the used fillers showed that the highest tensile stress was for 1Fe-Al<sub>2</sub>O<sub>3</sub>/EVA/UHMWPE.

The measured values of tensile strength for 1n-Al<sub>2</sub>O<sub>3</sub>/EVA/UHMWPE, 1w-Al<sub>2</sub>O<sub>3</sub>/EVA/UHMWPE and 1Fe-Al<sub>2</sub>O<sub>3</sub>/EVA/UHMWPE compared to EVA/UHMWPE showed an increase of 63.0%, 31.9% and 100.7%, respectively. The significant improvement in the mechanical properties could be attributed to the strong interaction

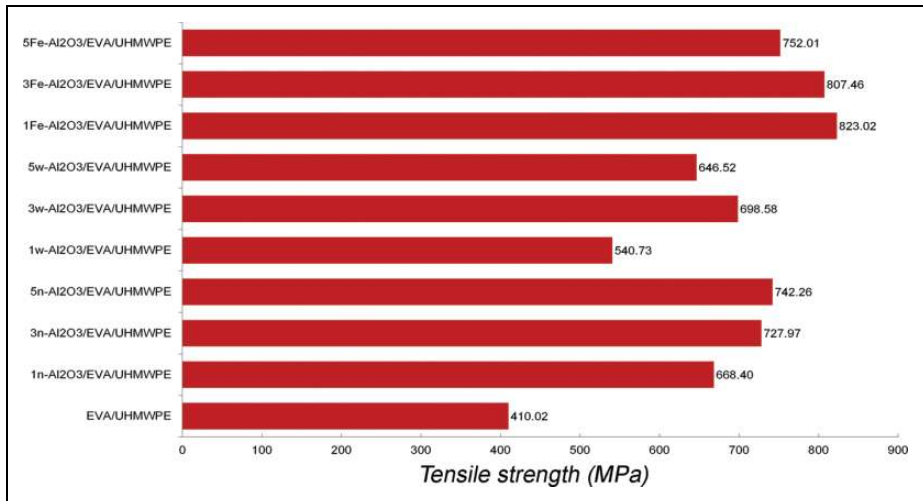


**Figure 9.** Tensile test results of hybrid composites.

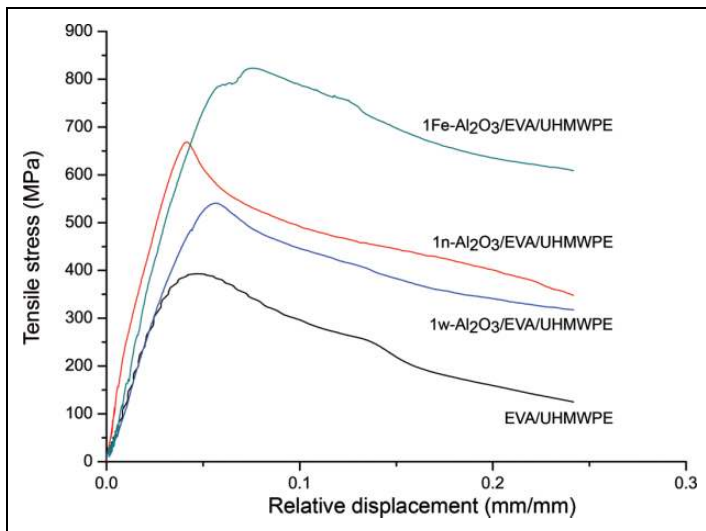


**Figure 10.** Tensile test diagram for hybrid composite fibres with 1 wt% of fillers.

between the hydroxyl groups of Fe-Al<sub>2</sub>O<sub>3</sub> and EVA because of the sintering process at lower temperatures, where OH groups partially remained on alumina surface, so the better binding with EVA was expected. Formation of agglomerates of w-Al<sub>2</sub>O<sub>3</sub> resulted in a reduction of tensile strength value.

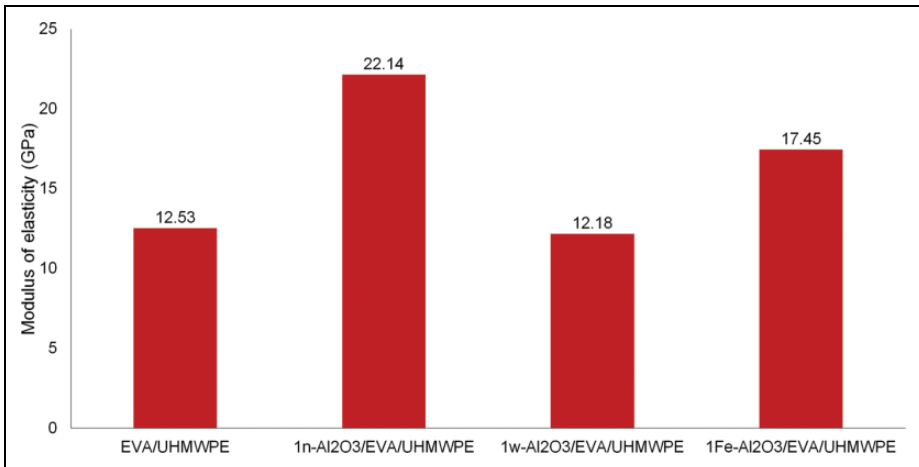


**Figure 11.** Effect of the composition of the samples on the modulus of elasticity.

Resulting values of the modulus of elasticity (Figure 11) had a different trend. The highest value of modulus of elasticity shown for 1n-Al<sub>2</sub>O<sub>3</sub>/EVA/UHMWPE indicated the increase of rigidity of the hybrid composites, resulting brittle failure of the matrix seen in the SEM image (Figure 5(a)). A larger area under the stress-displacement curve for the 1Fe-Al<sub>2</sub>O<sub>3</sub>/EVA/UHMWPE sample was a consequence of more resilient composite obtained that can absorb a higher amount of tensile energy. Such a behaviour was reflected by lower modulus of elasticity. Alumina fillers in a form of whiskers in a sample 1w-Al<sub>2</sub>O<sub>3</sub>/EVA/UHMWPE caused the lowest mechanical properties in relation to other hybrid composites, while the modulus of elasticity was lower than the one obtained for EVA without particle reinforcement (EVA/UHMWPE). This behaviour may be explained with higher amount of aggregates in the matrix that disabled interaction with the main reinforcement of the composites – UHMWPE.

## Conclusions

In this article, experimental results were presented for UHMWPE fibres as reinforcement with 1, 3 and 5 wt% of alumina nanoparticles, whiskers and iron doped alumina particles as fillers in EVA matrix. The tensile results obtained for hybrid composites with 1 wt% of particles indicated that the optimal weight percentage was used which was compliant with the literature.

In comparison with other used commercial fillers, Fe-Al<sub>2</sub>O<sub>3</sub> showed a submicron particle size distribution. Average diameter of 0.15 μm had a significant effect on the mechanical properties due to better dispersion and distribution in the matrix.

FE-SEM analysis proved the best fibre–matrix interfacial adhesion for 1-Fe-Al<sub>2</sub>O<sub>3</sub>/EVA/UHMWPE due to resilient longitudinal cracking of EVA that confirmed excellent bonding.



This was in agreement with tensile test results where 1-Fe-Al<sub>2</sub>O<sub>3</sub>/EVA/UHMWPE showed improved mechanical properties in comparison with hybrid composite fibres with nanoparticles or whiskers.

FTIR spectra indicated better interactions between Fe-Al<sub>2</sub>O<sub>3</sub> and matrix due to established hydrogen bonds.

Presented results from the FTIR, FE-SEM and tensile stress analysis showed that in comparison with commercially available aluminium oxide nanoparticles with particle size less than 50 nm and alumina whiskers (diameter 2–4 nm × 400 nm), synthesized iron oxide doped alumina particles were the best choice for hybrid reinforcement of EVA/UHMWPE composites.

DSC analysis presented the highest melting enthalpy of UHMWPE phase (32.3 J g<sup>-1</sup>) for 1Fe-Al<sub>2</sub>O<sub>3</sub>/EVA/UHMWPE, which indicated that the composite with the best structural arrangement of main reinforcement was obtained.

TG/DTG curves represented that the degradation process temperatures of EVA matrix, UHMWPE fibres and UHMWPE/EVA composites were similar for all samples except UHMWPE fibres. Temperature of onset of degradation ( $T_{0.05}$ ) showed that the particles improved the thermal stability of EVA/UHMWPE composites, where the highest value was observed for UHMWPE fibres. It was interesting to notice that iron doped particles improved the thermal stability of hybrid composite until 350°C even compared to UHMWPE fibres.

In general, the incorporation of different combinations of fillers had a significant improvement effect on the modulus of elasticity causing different types of composite failure. The highest modulus of elasticity for composite with alumina nanoparticles (1n-Al<sub>2</sub>O<sub>3</sub>/EVA/UHMWPE) was followed by brittle matrix failure. The most resilient hybrid composite with iron doped alumina represented the composite that was able to absorb the highest amount of tensile energy.

It can be concluded that EVA/UHMWPE hybrid composite fibres with Fe-Al<sub>2</sub>O<sub>3</sub> particles were superior to those of EVA/UHMWPE or hybrid composites with Al<sub>2</sub>O<sub>3</sub> nanoparticles or whiskers.

### **Acknowledgement**

The authors wish to acknowledge the financial support from the Ministry of Education, Science and Technological Development of the Republic of Serbia.

### **Declaration of Conflicting Interests**

The author(s) declared no potential conflicts of interest with respect to the research, authorship, and/or publication of this article.

### **Funding**

The author(s) disclosed receipt of the following financial support for the research, authorship, and/or publication of this article: This work received the financial support from the Ministry of Education, Science and Technological Development of the Republic of Serbia through project no. TR 34011.

## References

1. Lin SP, Han JL, Yeh JT, et al. Surface modification and physical properties of various UHMWPE-fiber-reinforced modified epoxy composites. *J Appl Polym Sci* 2007; 104: 655–665. DOI: 10.1002/app.25735
2. Razavi-Nouri M and Karami M. Effect of rubber content on morphology and thermal and rheological behaviors of acrylonitrile-butadiene rubber/poly(ethylene-co-vinyl acetate)/organoclay nanocomposites. *Polym (United Kingdom)* 2014; 55(26): 6940–6947. DOI: 10.1016/j.polymer.2014.10.050.
3. Cavodeau F, Sonnier R, Otazaghine B, et al. Ethylene-vinyl acetate copolymer/aluminium trihydroxide composites: a new method to predict the barrier effect during cone calorimeter tests. *Polym Degrad Stab* 2015; 120: 23–31. DOI: 10.1016/j.polymdegradstab.2015.05.021.
4. El Hage R, Viretto A, Sonnier R, et al. Flame retardancy of ethylene vinyl acetate (EVA) using new aluminum-based fillers. *Polym Degrad Stab* 2014; 108: 56–67. DOI: 10.1016/j.polymdegradstab.2014.05.029.
5. Chalykh AE, Stepanenko VY, Shcherbina AA, et al. Adhesive properties of ethylene and vinyl acetate copolymers. *Polym Sci Ser D* 2009; 2(1): 8–15. DOI: 10.1134/S199542120901002X.
6. Sviridenok AI, Zharin AL, Krautsevich AU, et al. The effect of high-dispersion fillers on adhesive and frictional properties of ethylene-vinyl acetate copolymer. *J Frict Wear* 2014; 35(4): 255–262. DOI: 10.3103/S1068366614040114.
7. Shi XM, Zhang J, Jin J, et al. Non-isothermal crystallization and melting of ethylene-vinyl acetate copolymers with different vinyl acetate contents. *Express Polym Lett* 2008; 2(9): 623–629. DOI: 10.3144/expresspolymlett.2008.75.
8. Soto Puente JA, Fatyeyeva K, Marais S, et al. Multifunctional hydrolyzed EVA membranes with tunable microstructure and water barrier properties. *J Memb Sci* 2015; 480: 93–103. DOI: 10.1016/j.memsci.2015.01.008.
9. Zhang Y, Gu J, Tan H, et al. Preparation and characterization of film of poly vinyl acetate ethylene copolymer emulsion. *Appl Surf Sci* 2013; 276: 223–228. DOI: 10.1016/j.apsusc.2013.03.071.
10. Kango S, Kalia S, Celli A, et al. Surface modification of inorganic nanoparticles for development of organic-inorganic nanocomposites – A review. *Prog Polym Sci* 2013; 38(8): 1232–1261. DOI: 10.1016/j.progpolymsci.2013.02.003.
11. Marissen R. Design with ultra strong polyethylene fibers. *Mater Sci Appl* 2011; 2(May): 319–330. DOI: 10.4236/msa.2011.25042.
12. Chang BP, Md. Akil H and Bt. Md. Nasir R. Comparative study of micro- and nano-ZnO reinforced UHMWPE composites under dry sliding wear. *Wear* 2013; 297(1–2): 1120–1127. DOI: 10.1016/j.wear.2012.11.083.
13. Hsieh AJ, Chantawansri TL, Hu W, et al. New insight into the influence of molecular dynamics of matrix elastomers on ballistic impact deformation in UHMWPE composites. *Polym (United Kingdom)* 2016; 95: 52–61. DOI: 10.1016/j.polymer.2016.04.048.
14. McDaniel PB, Deitzel JM and Gillespie JW. Structural hierarchy and surface morphology of highly drawn ultra high molecular weight polyethylene fibers studied by atomic force microscopy and wide angle X-ray diffraction. *Polymer* 2015; 69: 148–158. DOI: 10.1016/j.polymer.2015.05.010.
15. Kang YA, Oh SH and Park JS. Properties of UHMWPE fabric reinforced epoxy composite prepared by vacuum-assisted resin transfer molding. *Fibers Polym* 2015; 16(6): 1343–1348. DOI: 10.1007/s12221-015-1343-8.

16. Chand N, Dwivedi UK and Sharma MK. Development and tribological behaviour of UHMWPE filled epoxy gradient composites. *Wear* 2007; 262(1–2): 184–90. DOI:10.1016/j.wear.2006.04.012.
17. Oliveira M and Machado AV. Preparation and characterization of ethylene-vinyl acetate nanocomposites: enhanced flame retardant. *Polym Int* 2013; 62(12): 1678–1683. DOI: 10.1002/pi.4466.
18. Jin B, Zhang W, Sun G, et al. Fabrication and characterization of ethylene-vinyl acetate copolymer/Al<sub>2</sub>O<sub>3</sub> nanocomposites. *J Ceram Process Res* 2007; 8(5): 336–340.
19. Baskaran R, Sarojadevi M and Vijayakumar CT. Unsaturated polyester nanocomposites filled with nano alumina. *J Mater Sci* 2011; 46(14): 4864–4871. DOI: 10.1007/s10853-011-5398-7.
20. Chee CY, Song NL, Abdullah LC, et al. Characterization of mechanical properties: low-density polyethylene nanocomposite using nanoalumina particle as filler. *J Nanomater* 2012; 2012: 6. DOI:10.1155/2012/215978.
21. Mallakpour S and Khadem E. Recent development in the synthesis of polymer nanocomposites based on nano-alumina. *Prog Polym Sci* 2014; 51: 74–93. DOI: 10.1016/j.progpolymsci.2015.07.004.
22. Milanović P, Dimitrijević M, Jančić Heinemann R, et al. Preparation of low cost alumina nanofibers via electrospinning of aluminium chloride hydroxide/poly (vinyl alcohol) solution. *Ceram Int* 2013; 39(2): 2131–2134. DOI: 10.1016/j.ceramint.2012.07.062.
23. Opelt CV, Becker D, Lepienski CM, et al. Reinforcement and toughening mechanisms in polymer nanocomposites – Carbon nanotubes and aluminium oxide. *Composites Part B* 2015; 75: 119–126. DOI: 10.1016/j.compositesb.2015.01.019.
24. Wetzal B, Rosso P, Hauptert F, et al. Epoxy nanocomposites – fracture and toughening mechanisms. *Eng Fract Mech* 2006; 73(16): 2375–2398. DOI: 10.1016/j.engfracmech.2006.05.018.
25. Cho J, Joshi MS and Sun CT. Effect of inclusion size on mechanical properties of polymeric composites with micro and nano particles. *Compos Sci Technol* 2006; 66(13): 1941–1952. DOI: 10.1016/j.compscitech.2005.12.028.
26. Opelt CV and Coelho LAF. Reinforcement and toughening mechanisms in polymer nanocomposites – reinforcement effectiveness and nanoclay nanocomposites. *Mater Chem Phys* 2015; 169: 179–185. DOI: 10.1016/j.matchemphys.2015.11.047.
27. Heydari-Meybodi M, Saber-Samandari S and Sadighi M. A new approach for prediction of elastic modulus of polymer/nanoclay composites by considering interfacial debonding: experimental and numerical investigations. *Compos Sci Technol* 2015; 117: 379–385. DOI: 10.1016/j.compscitech.2015.07.014.
28. Alzarrug FA, Dimitrijević MM, Jančić Heinemann RM, et al. The use of different alumina fillers for improvement of the mechanical properties of hybrid PMMA composites. *Mater Des* 2015; 86: 575–581. DOI: 10.1016/j.matdes.2015.07.069.
29. Tomić NZ, Međo BI, Stojanović DB, et al. A rapid test to measure adhesion between optical fibers and ethylene–vinyl acetate copolymer (EVA). *Int J Adhes Adhes* 2016; 68: 341–350. DOI: 10.1016/j.ijadhadh.2016.04.012.
30. An M, Xu H, Lv Y, et al. Ultra-strong gel-spun ultra-high molecular weight polyethylene fibers filled with chitin nanocrystals. *RSC Adv* 2016; 6(25): 20629–20636. DOI: 10.1039/C5RA25786G.
31. Stark W and Jaunich M. Investigation of ethylene/vinyl acetate copolymer (EVA) by thermal analysis DSC and DMA. *Polym Test* 2011; 30(2): 236–242. DOI: 10.1016/j.polymertesting.2010.12.003.

32. Badiee A, Ashcroft IA and Wildman RD. The thermo-mechanical degradation of ethylene vinyl acetate used as a solar panel adhesive and encapsulant. *Int J Adhes Adhes* 2016; 68: 212–218. DOI: 10.1016/j.ijadhadh.2016.03.008.
33. Marín ML, Jiménez A, López J, et al. Thermal degradation of ethylene (vinyl acetate) kinetic analysis of thermogravimetric data. *J Therm Anal* 1996; 47(1): 247–258. DOI: 10.1007/BF01982703.
34. Osayemwenre GO and Meyer EL. Thermal decomposition of EVA composite encapsulant of single junction amorphous silicon photovoltaic (PV) module. *J Ovonic Res* 2014; 10(6): 221–229.
35. Lizymol PP and Thomas S. Thermal behaviour of polymer blends: a comparison of the thermal properties of miscible and immiscible systems. *Polym Degrad Stab* 1993; 41(1): 59–64. DOI: 10.1016/0141-3910(93)90061-M.
36. Mochane MJ and Luyt AS. The effect of expanded graphite on the thermal stability, latent heat, and flammability properties of EVA/wax phasechange blends. *Polym Eng Sci* 2015; 25: 1255–1262. DOI: 10.1002/pen.24063.
37. Costache MC, Jiang DD and Wilkie CA. Thermal degradation of ethylene-vinyl acetate copolymer nanocomposites. *Polymer* 2005; 46(18): 6947–6958. DOI: 10.1016/j.polymer.2005.05.084.